Imaging the rotationally state-selected NO(A,n) product from the predissociation of the A state of the NO-Ar van der Waals cluster

Roeterdink, W.G.; Strecker, K.E.; Hayden, C.C.; Janssen, M.H.M.; Chandler, D.W.

published in
Journal of Chemical Physics
2009

DOI (link to publisher)
10.1063/1.3078773

document version
Publisher's PDF, also known as Version of record

Imaging the rotationally state-selected NO(A,n) product from the predissociation of the A state of the NO–Ar van der Waals cluster

Wim G. Roeterdink,[1,2] Kevin E. Strecker,[1] Carl C. Hayden,[1] Maurice H. M. Janssen,[2] and David W. Chandler[1,a)]

[1]*Sandia National Laboratories, Combustion Research Facility, Livermore, California 94550, USA*
[2]*Department of Chemistry and Laser Centre, Vrije Universiteit, de Boelelaan 1083, 1081 HV Amsterdam, The Netherlands*

(Received 19 May 2008; accepted 16 January 2009; published online 1 April 2009)

The origin of the resonant structures in the spectrum of the predissociative part of the A state in the NO–Ar van der Waals cluster has been investigated. We have employed direct excitation to the predissociative part of the NO–Ar A state followed by rotational state selective ionization of the NO fragment. Velocity map imaging of the NO ion yields the recoil energy of the rotational state-selected fragment. A substantial contribution of rotational hotbands to the resonant structures is observed. Our data indicate that a centrifugal barrier as the origin of these resonances can be ruled out. We hypothesize that after the NO–Ar cluster is excited to the A state sufficient mixing within the rotating cluster takes place as it changes geometry from being T shaped in the NO(X)–Ar state to linear in the NO(A)–Ar state. This mixing allows the low energy and high angular momentum ($J \approx 4.5$) tumbling motion of the initially populated hotbands in the ground state NO(X)–Ar complex to be converted into NO($A,n=2$) spinning rotation in the A state of the complex. The electronically excited spinning complex falls apart adiabatically producing rotationally excited NO($A,n=2$) at the energetic threshold. This interpretation indicates that the resonances can be attributed to some type of vibrational Feshbach resonance. The appearance energy for the formation of NO($A,n=0$)+Ar is found to be 44294.3 ± 1.4 cm^{-1}. © *2009 American Institute of Physics*. [DOI: 10.1063/1.3078773]

I. INTRODUCTION

The interaction between the rare gas atom Ar and the open shell molecule NO has been extensively studied employing crossed beam scattering experiments,[1,2] photodissociation of the NO–Ar van der Waals complex,[3,4] and spectroscopy.[5–10] The scattering experiments performed typically have a high collision energy ~500 cm^{-1} above the NO(X)+Ar asymptote and the agreement with *ab initio* calculations[1,2,11] suggests that there is a good understanding of the interaction and dynamics involved, i.e., scattering from the repulsive part of the potential energy surface at these energies. Nonresonant photodissociation of the NO–Ar complex has been performed at a range of energies above the NO(A)+Ar asymptote, typically 25–400 cm^{-1}. The rotational energy distribution found in the NO(A) fragment peaks near the highest rotational state which is energetically accessible. This can be attributed to the rotational rainbow effect.[3,4] However, no unambiguous conclusion could be drawn about the presence of a barrier for dissociation due to the possible presence of rotational hotbands. Spectroscopy on the van der Waals complexes gives detailed information on the ground and excited state potential energy surfaces, in particular, the bound region and the repulsive inner region of the potential energy surfaces.[10,12] These spectroscopic studies have shown that NO(X)–Ar, i.e., the electronic ground state is nearly T shaped. The A state of the NO–Ar cluster has been studied using resonance-enhanced multiphoton (REMPI) techniques[5–7] and laser induced fluorescence.[8,13] It was found that the vibrational ground state of the electronically excited NO(A)–Ar is nearly linear, however, the vibrationally excited states show a skewed T shape structure.

In order to study the long-range, attractive part of the potential energy surface one needs to do an experiment that is sensitive to this part of the potential, typically 0–50 cm^{-1} above the NO(A)+Ar asymptote. Near threshold photodissociation of the van der Waals complex can, in principle, reveal typical features of cold collisions such as shape and Feshbach resonances.[14] Low energy scattering cross sections are usually dominated by shape resonances due to small centrifugal barriers at relatively large internuclear distances. Similar resonance-like features have been found in the NO–Ar cluster above the NO(A)+Ar dissociation asymptote. Miller was the first to report these above threshold resonances in NO–Ar cluster using (1+1) multiphoton ionization, however, no possible assignment of the peaks could be given.[15] Later, McQuaid *et al.*[6] and Tsuji *et al.*[5] also found predissociative bound-bound $A \leftarrow X$ transitions in the NO–Ar complex, ~25 cm^{-1} above the NO(A)+Ar dissociation asymptote. Previously, shape resonances were observed in the very weakly bound (7.1 cm^{-1}) HF–Ne van der Waals cluster.[16] The excitation of the two-dimensional bend-stretch vibrations in the van der Waals complex can give rise to a hindered rotation of the diatom in the plane of the complex,

a)Author to whom correspondence should be addressed. Electronic mail: chand@sandia.gov.

the so called free rotor state, which is well above the dissociation threshold. Such resonant structures were observed in the OH–Ar van der Waals complex which were coupled to the continuum through vibrational predissociation.[17]

Tsuji *et al.*[5] employed a two-color REMPI scheme to study the NO–Ar cluster: a photon slightly blueshifted from the free NO A-X transition excites and dissociates the NO–Ar complex to produce NO in the electronic A state, NO(A), and an argon atom. The NO(A) molecules are subsequently resonantly ionized through the E state, using a second laser which selects a rotational quantum state, labeled n. Both the groups of Tsuji and McQuaid tentatively assigned the resonances in terms of rotational transitions to a van der Waals stretch-bend vibration combination band. Theoretically it has been shown that a (half) collision between a rare gas atom and a vibrationally excited diatomic molecule can give rise to vibrational Feshbach resonances.[18,19] A vibrational Feshbach resonance is a resonance of a system which would turn into a bound state when the coupling between the internal degrees of freedom in the van der Waals cluster and the degrees of freedom associated with the fragments were set to zero. The coupling term in the theoretical model is introduced by an asymmetric coupling between the two orthogonal bend and stretch vibrations.

Several experiments have determined the appearance energy of NO(A,n=0)+Ar from the NO(X)–Ar complex. Tsuji *et al.*[5] reported an appearance energy for the NO(A,n=0) of $44\,286.7 \pm 0.3$ cm^{-1}. This value was obtained under the assumption that there is no contribution from rotationally and vibrationally excited NO(X)–Ar clusters. Later, Parsons *et al.*[3] used nonresonant dissociation followed by resonant ionization to determine the distribution of the NO(A) fragments into the different rotational channels, 25–400 cm^{-1} above the NO(A)+Ar dissociation energy. They reported the appearance energy for NO(A,n=0) to be $44\,291 \pm 2$ cm^{-1}. An appearance energy of $44\,294 \pm 2$ cm^{-1} was calculated from the well depth determined in the scattering experiments by Thuis *et al.*[20]

The presence of rotationally hot, and higher order clusters has been a recurring subject in previous studies: Parsons *et al.*[3] observed possible hotband contributions.[3] Bush *et al.*[7,15] reported that they could not reproduce Miller[15] spectrum by systematically varying their expansion conditions. Shafizadeh *et al.*[8] showed that there are clear broad underlying features in the spectra which they attribute to larger complexes. Understanding the effects of rotational hotbands upon the dissociation dynamics underlies the discrepancies in the threshold measurements. In general, it is very difficult to produce a molecular beam solely consisting of NO(X)–Ar(P'=0.5) complexes, where P' is the projection of the total rotational angular momentum J' on the NO–Ar axis.[10]

In this study we combine the double-resonant dissociation/ionization approach of Tsuji with velocity map ion imaging of the products.[21,22] The high selectivity of the $E \leftarrow A$ spectroscopy combined with the determination of the kinetic energy of the products makes it possible to determine the contributions of rotationally excited states of the NO(X)–Ar cluster. We report the first measurement of the velocity distribution of the NO(A) product molecules following excitation to the predissociative resonances.

II. EXPERIMENTAL

The molecular beam consists of NO seeded in argon and neon and is expanded through a homebuilt piezo valve with an orifice of 1 mm.[23] The molecular beam is singly skimmed by a 700 μm skimmer 50 mm downstream of the piezo valve. The backing pressure, timing of the piezo valve and the seeding fraction were optimized on the observed resonances of the $A \leftarrow X$ transition. A mixture of 2% NO, 48% Ar, and 50% Ne was used, with a stagnation pressure of 2 bars. These conditions were found to give the sharpest rings in the ion images.

The second harmonic of the seeded Nd:YAG (yttrium aluminum garnet) is used to pump a Spectra Physics Sirah dye laser (0.03 cm^{-1} bandwidth, 30 Hz) to produce light around 620 nm which is mixed with the third harmonic of the seeded Nd:YAG laser (0.0003 cm^{-1} bandwidth) yielding light around 225.78 nm. This laser light excites the NO(X)–Ar complex above the NO(A)+Ar dissociation energy. Part of the second harmonic of the seeded Nd:YAG is split off to pump a second dye laser, the Lambda Physik Scanmate 2 (0.8 cm^{-1} bandwidth), to produce light around 600 nm to excite the $E \leftarrow A$ transition of the NO(A) products. This probe laser light selectively ionizes a specific rotational state of NO(A). The wavelength of the pump laser was determined using a wavemeter. Both laser beams are focused to $\sim$200 μm to ensure a good velocity resolution in the ion images. The velocity resolution is optimized by double-resonant ionization ($X \rightarrow A \rightarrow E \rightarrow$ ion) of free NO entrained in the molecular beam and then imaging the NO$^+$ onto the detector in a manner that gives the smallest image, 4 pixel [full width at half maximum (FWHM)]. The velocity resolution is measured to be $\sim$7 m/s pixel. For a (1+1′) REMPI transition in the NO molecule the recoil energy of the electron is close to this velocity resolution. The repeller and extractor are spaced 40 mm apart and placed at a 110 V difference. A third electrode at 30 mm from the extractor is used to focus the ions onto the micro-channel-plate (MCP). The MCP is shielded from the third electrode by an additional, grounded electrode, placed 30 mm from the third electrode. The total length of the time-of-flight (TOF) tube amounts to 650 mm and results in a total TOF of 14.33 μs for the NO ions. The typical voltages employed are the repeller at 500 V, the extractor at 390 V, and the lens at 300 V. The output of the phosphor is imaged on a charge-coupled device camera (LaVision 640$\times$480 pixels), to record the position of the NO ions. When taking data, a pair of polarizers in combination with a $\lambda/2$ plate is used to control the intensity of the dissociation laser such that only a few background NO ions per shot are made when only the dissociation laser is present. The ionization laser is spatially overlapped with the dissociation laser with a temporal delay of 12 ns. The observed kinetic energy distributions and angular distributions of the NO ions were found to be independent of the temporal delay between the pump and the probe laser. Typically around ten ions are made per laser shot. To obtain good data

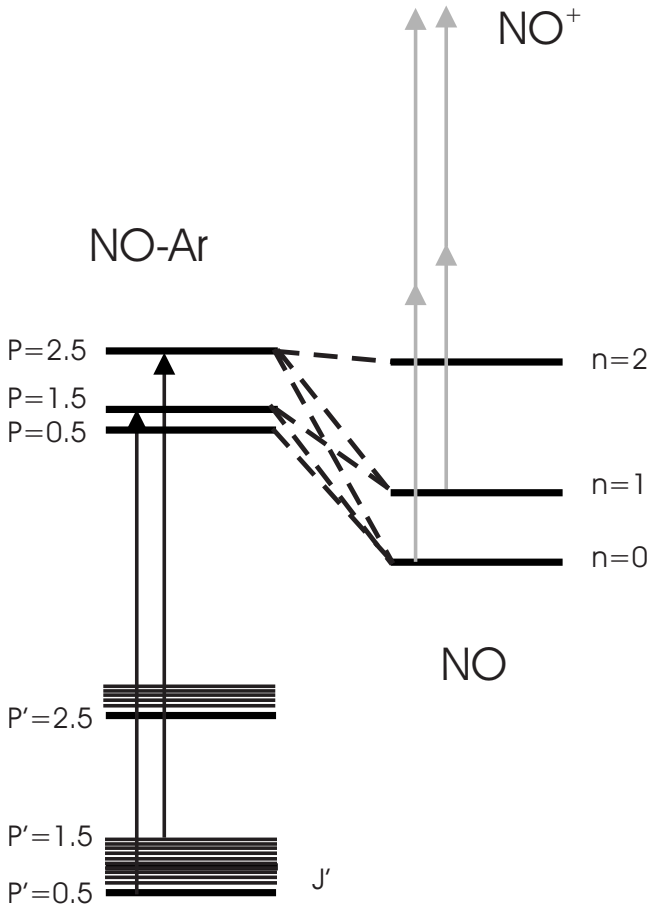

FIG. 1. Schematic level scheme of the NOAr cluster. The J' sublevels of the $P'=0.5$ and $P'=1.5$ levels of the NO(X)Ar state overlap. Exact energy levels can be found in Ref. 10. Excitation scheme: the pump laser excites the NO(X)–Ar(J',P') to the NO(A)–Ar(J,P) cluster. The NO(A)–Ar(J,P) cluster dissociates in NO(A,n)+Ar. The NO(A,n) molecule is rotationally state selectively ionized using a second laser.

images typically a background image and signal plus background image are averaged for 20 min before subtraction.

III. RESULTS AND DISCUSSION

A. Pump laser dissociation spectra

The laser excitation scheme is depicted in Fig. 1. A photon, blueshifted from the bare NO A-X transition, dissociates the NO(X)–Ar cluster to produce NO in the electronically excited A state and an argon atom. The NO(A,n) fragment is subsequently resonantly ionized through the E state by a probe laser, which selects a single rotational quantum state, labeled n. To distinguish between the quantum numbers of the bare NO molecule and the NO–Ar cluster we follow Kim *et al.*[10] and use small letter n to label the rotational states of the bare NO(A,n) molecule.

In Fig. 2 we show three pump laser dissociation spectra, labeled with $n=0$, 1, and 2, in which the pump laser is scanned and the probe laser was fixed at a particular wavelength to ionize a specific rotational quantum state of the NO(A,n) fragment. The fourth spectrum in Fig. 2 was taken with only the pump laser present. Very sharp lines are observed in Fig. 2 and they are attributed to ionization of NO(X,n) molecules from the thermal background by the

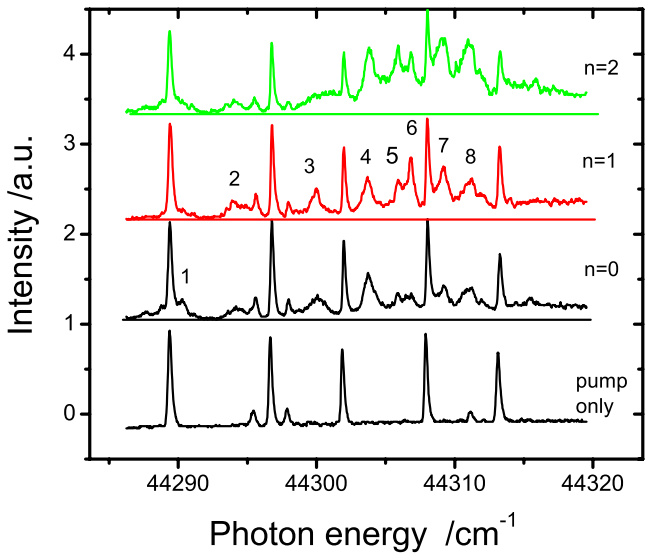

FIG. 2. (Color online) Photodissociation action spectra of the NO(X)–Ar cluster. The lowest trace shows the spectrum observed with the pump laser only and the probe laser blocked detecting "hot" NO in the background. The other traces are recorded in combination with the probe laser ionizing NO(A,n) molecules in the specified rotational state. The excitation scheme is depicted in Fig. 1. The transitions originating from the NO–Ar clusters are labeled with Nos. 1–8.

pump laser only. These sharp lines have no dependence on the probe laser and their frequencies and intensities correspond well with the frequencies and intensities found by Tsuji *et al.*[5] The energy of the pump photon is used as the horizontal axis of Fig. 2 and was calibrated using a wavemeter. Both NO ($A\ ^2\Sigma^+$) and NO ($E\ ^2\Sigma^+$) belong to Hund's case B angular momentum coupling scheme where the spin angular momentum is decoupled from the internuclear axis. The good quantum number for the NO(A) and NO(E) electronic states is $n=j\pm 1/2$.

The resonant structures between the sharp lines have a pump-probe dependence and originate from NO–Ar clusters. These broadened peaks have a FWHM of about $\Delta\nu=2\ \mathrm{cm}^{-1}$. It is unclear from previous studies what the exact origin of these above threshold resonances is, although Tsuji *et al.*[5] assumed a centrifugal barrier. In the following sections we will analyze and discuss ion images taken at various combinations of pump and probe wavelengths to reveal the origin of the above threshold resonances.

B. Ion imaging

Ion imaging measures the kinetic energy and the angular distribution of the produced NO(A,n) fragment by imaging its velocity. Because of the conservation of energy and linear momentum, the NO(A,n) fragments originating from dissociation of the NO–Ar cluster will show up as a ring in the ion images. Because of the experimental geometry with the polarizations of pump and probe lasers parallel to the detector plane the experimental two-dimensionally projected velocity map ion images can be inverted to three-dimensional ion images using Abel-inversion techniques. Figure 3 shows three Abel-inverted images with the pump laser set at a fixed wavelength, labeled as transition 7 in Fig. 2, and the probe laser set at three different rotational states of the NO(A,n)

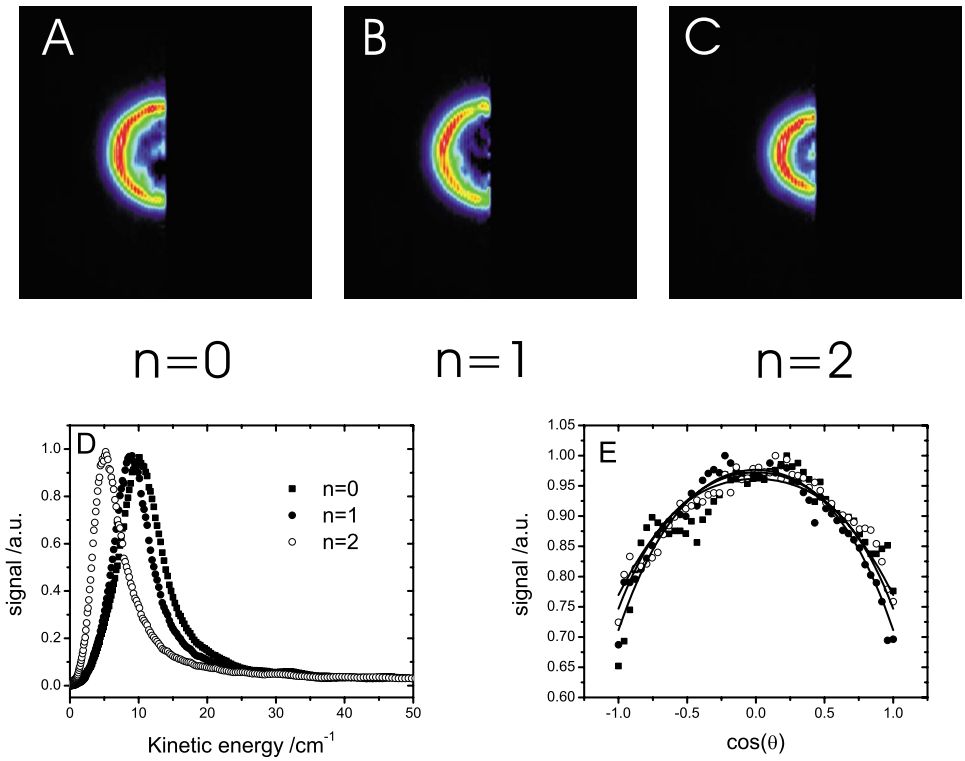

FIG. 3. (Color online) [(A)–(C)] Abel-inverted ion images obtained for transition 7 for $n=0$, 1, and 2. (D) Kinetic energy distribution of the NO^+ fragment derived from the ion images above. Note that the transients are normalized and do not reflect the branching ratios. (E) Angular distributions of the NO^+ fragment.

fragment, $n=0$, 1, and 2. In Fig. 4 we present similar images with the pump laser fixed at a wavelength labeled as transition 5 in Fig. 2.

The NO^+ ions, produced by ionization of $NO(A,n)$ fragments from dissociation of the $NO(X)-Ar$ cluster, appear as a clear ring in the ion images of Figs. 3 and 4. We do not believe that there is a substantial contribution of $NO(A,n)$ fragments from dissociation of larger $NO-Ar_m$ $(m>1)$ clusters. At these near threshold energies with such a small amount of excess energy it is not possible to break an Ar–Ar van der Waals bond but excitation of rotational and vibrational states of a Ar_m cluster would give rise to lower velocity NO fragments. Moreover, this would give rise to a continuous distribution of $NO(A,n)$ fragments with lower recoil energies, i.e., dissociation of larger $NO-Ar_m$ $(m>1)$ clusters would give intensity inside the ring. We do not observe such

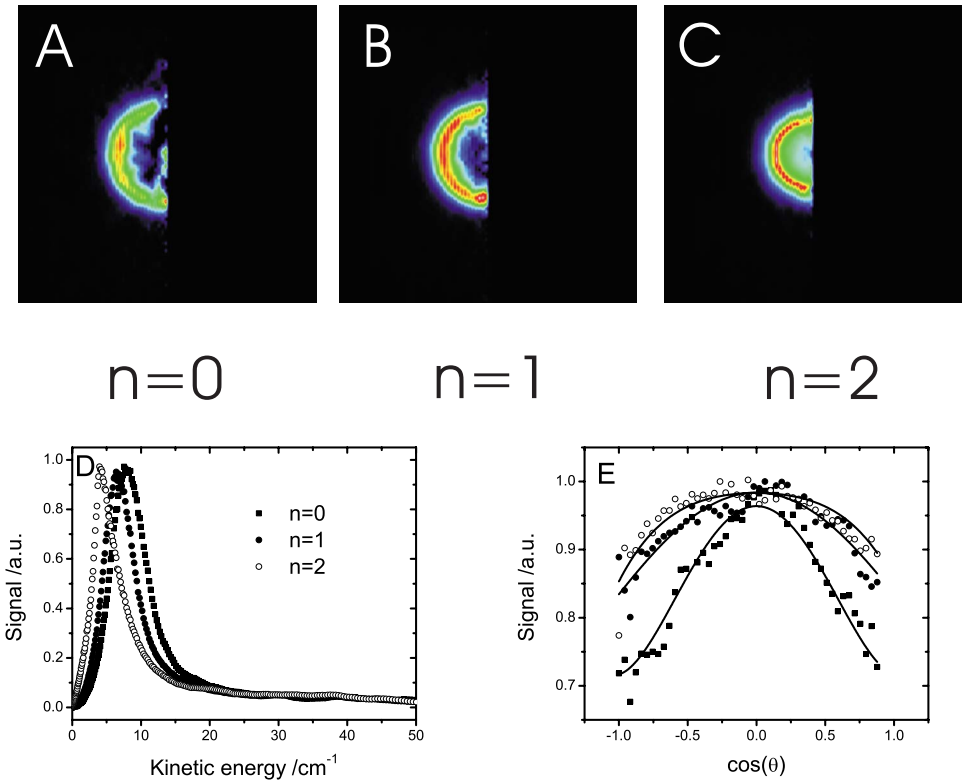

FIG. 4. (Color online) [(A)–(C)] Abel-inverted ion images obtained for transition 5 for $n=0$, 1, and 2. (D) Kinetic energy distribution of the NO^+ fragment derived from the ion images above. Note that the transients are normalized and do not reflect the branching ratios. (E) Angular distributions of the NO^+ fragment.

TABLE I. The energetics of the NO(A,n)+Ar dissociation derived from the ion images.

Peak	E_{photon} (cm^{-1})	n	$E_{kin,tot,peak}$ (cm^{-1})	$E_{kin,tot}$ (cm^{-1})	E_{rot} (cm^{-1})	$E_{int,cluster}$ (cm^{-1})	Width (cm^{-1})	β
1	44 291.0	0	2.6	0.1	0	3.2	5.1	⋯
2	44 294.0	0	3.5	0.8	0	2.1	5.4	⋯
		1	1.1	0.1	4	5.2	2.0	⋯
3	44 300.0	0	10.9	7.7	0	2.0	6.5	−0.13
		1	8.4	5.3	4	3.6	6.2	−0.17
4	44 303.5	0	12.7	8.9	0	−0.3	7.6	−0.15
		1	9.5	5.7	4	1.1	7.6	−0.15
		2	4.7	2.0	12	3.8	5.4	−0.08
5	44 304.0	0	13.6	9.5	0	−0.2	8.2	−0.23
		1	11.5	8.0	4	2.3	7.0	−0.15
		2	6.8	3.7	12	6.0	6.2	−0.17
6	44 307.0	0	15.9	11.5	0	−1.2	8.8	−0.21
		1	11.3	7.3	4	−1.4	8.0	−0.17
		2	8.0	4.5	12	3.8	7.0	−0.11
7	44 309.5	0	18.6	14.0	0	−1.2	9.3	−0.16
		1	16.8	12.9	4	1.7	7.9	−0.21
		2	8.3	5.2	12	2.0	6.2	−0.17
8	44 311.0	0	22.2	17.1	0	0.4	10.3	−0.16
		1	18.7	13.8	4	1.1	9.9	−0.20
		2	10.2	6.1	12	1.4	8.2	−0.06

a background at low kinetic energy and therefore we believe the contribution of NO(A,n) fragments from dissociation of NO–Ar_m ($m>1$) clusters is negligible.

Comparing the images in Figs. 3 and 4 for different final rotational states $n=0$, 1, and 2 we observe that the amount of kinetic energy is clearly smaller when more energy is distributed as rotational energy in the NO(A,n) fragment. This is reflected by the smaller diameter of the ring in the ion images with increasing rotational level n. Conservation of energy and linear momentum dictates that the total kinetic energy of the dissociation, $E_{kin,tot}$, can be extracted from the experimentally determined kinetic energy of NO(A,n) fragment as follows:

$$E_{kin,tot} = E_{kin,NO}\left(1 + \frac{m_{NO}}{m_{Ar}}\right). \quad (1)$$

The appearance energy, E_{app}, the minimal energy required to observe NO(A,$n=0$), can now be calculated using the following relation:

$$E_{int,cluster} + E_{pump\ photon} = E_{kin,tot} + E_{rot,NO(A,n)} + E_{app}. \quad (2)$$

In this experiment we measure $E_{kin,tot}$, at a known pump photon energy, $E_{pump\ photon}$, for a selected final rotational state of the NO(A,n) fragment with rotational energy $E_{rot,NO(A,n)}$. This means that the two unknown energies in Eq. (2) are $E_{int,cluster}$ and the appearance energy E_{app}.

Equation (2) is solved for each detected NO(A,n) rotational state as follows. First the total kinetic energy was extracted from the ion images for the three rotational fragment channels NO(A,$n=0,1,$and2), at eight different dissociation energies $E_{pump\ photon}$, which are listed in Table I in the column labeled $E_{kin,tot,peak}$. Assuming now that the NO(A,$n=0$) fragments result from dissociation of NO(X)–Ar clusters with the smallest amount of internal energy we calculate E_{app} for the $n=0$ rotational channel using Eq. (2) with $E_{int,cluster}=0$. The velocity of the rising edge of the velocity distribution corresponds to the minimal kinetic energy of a particular NO(A,$n=0$) channel. Higher velocities are attributed to NO formed from a rotationally hot cluster. After we do this using all measured values for $n=0$ transitions we find that our value of the appearance energy means that peaks 1, 2, and 4 of Fig. 2 are hotband transitions. We therefore recalculate the appearance energy using only the $n=0$ transitions that do not arise from hot bands. This calculation gives us a value of $E_{app}=44\,294.3\pm1.4\ cm^{-1}$. The width of the kinetic energy distributions is listed in Table I in the column labeled width. These widths correspond with an approximate rotational temperature of 7.5 K and compare very well with the rotational temperature found by Bush *et al.*[7] who used similar expansion conditions. Note that the product of the stagnation pressure and the nozzle diameter in our experiment and the experiment of Bush *et al.* are identical. From the average of the calculation of the appearance energy for the NO($n=0$) fragment on transitions 3 and 5–8 we obtain $E_{app}=44\,294.3\pm1.4\ cm^{-1}$. This value is in excellent agreement with the value of $44\,294\pm2\ cm^{-1}$ derived from the NO Ar scattering experiment of Thuis *et al.*[20] The appearance energy derived from the data by Thuis *et al.* was calculated by using the well depth determined in the scattering experiment and adding the energy of the NO(A) band origin. Adding the energy of the band origin prevents problems with the zero point energy. Parsons *et al.*,[3] derived a value of $44\,291\pm2\ cm^{-1}$ but hotband contributions could not be ruled out. Tsuji *et al.* derived a value of $44\,286.7\pm0.3$ also under the assumption that there are no hotband contributions.[5] However, this appearance energy of

44 286.7 cm^{-1} would have the consequence that the slowest NO ions would have a kinetic energy which is approximately 7 cm^{-1} higher than our observation.

The appearance energy, E_{app}, is assumed to represent the dissociation of a NO(X)–Ar cluster from the rotational ground state, $P'=1/2$, with P' the projection of the total rotational angular momentum J' on the NO–Ar axis. In a joint theoretical and experimental study of lower bound states of NO(X)–Ar, the $P'=1.5$ state was found to have an energy of 3.5 cm^{-1} and the $P'=2.5$ state was found to have an energy of 10.6 cm^{-1} above the $P'=0.5$ state.[10] The rotational constant of the J' manifold for the NO(X)–Ar cluster is approximately 0.07 cm^{-1}.[7] The J' level spacing of NO(X)–Ar is small compared to the energy resolution of our ion imaging detector and cannot be resolved. A small increase in the width of the kinetic energy distribution can be observed with increasing excess energy, which is attributed to the fact that more J' levels contribute to signal at higher excess energy, see Table I.

Using the value of the appearance energy $E_{app}=44\,294.3$ cm^{-1}, the minimal values of $E_{int,complex}$ can be calculated for all NO($A,n=1,2$) fragment channels by energy conservation using Eq. (2). These values are also listed in Table I. A positive value of $E_{int,complex}$ indicates a surplus of internal rotational energy, which means that the transition originates from an excited rotational state in the NO(X)–Ar cluster. A surplus of 3.5 cm^{-1} indicates that the transition energetically is capable of originating from the NO(X)–Ar $P'=1.5$ level and a surplus of 10.6 cm^{-1} indicates that the transition is energetically capable of originating from the $P'=2.5$ level. Excess energy on the order of 3–5 cm^{-1} are observed for production of some of the NO($A,n=2$) products.

The internal energies listed in Table I suggest that mainly the rotational levels $P'=0.5$ and 1.5 of the NO(X)–Ar van der Waals cluster are present in the expansion. On average the total internal energy is found to be $\langle E_{int,complex}\rangle \approx 1.8$ cm^{-1}. Assuming a rotational constant of the NO(X)Ar cluster of 0.07 cm^{-1} this corresponds to a rotational quantum number of the cluster of about J' max 4.5. The centrifugal barrier height related to this rotation level can be estimated with

$$E_{barrier}=\frac{J(J+1)\hbar^2}{2\mu r^2}, \tag{3}$$

with μ as the reduced mass of the NO–Ar cluster and r as the distance between the center of mass of the NO molecule and the argon atom. r is assumed to be 3.6 Å, the equilibrium distance of the NO(X)–Ar cluster. The barrier height found for the $J=4.5$ rotational level is $E_{barrier}\approx 1.8$ cm^{-1}. In Table I we observe that the kinetic energy of the departing NO(A,n) molecule ranges from 7.7 cm^{-1} at the transition labeled 3–17.1 cm^{-1} at the transition labeled 8. This kinetic energy is significantly larger than the estimated centrifugal barrier energy of 1.8 cm^{-1}, and indicates that the observed resonance structures do not originate from a centrifugal barrier.

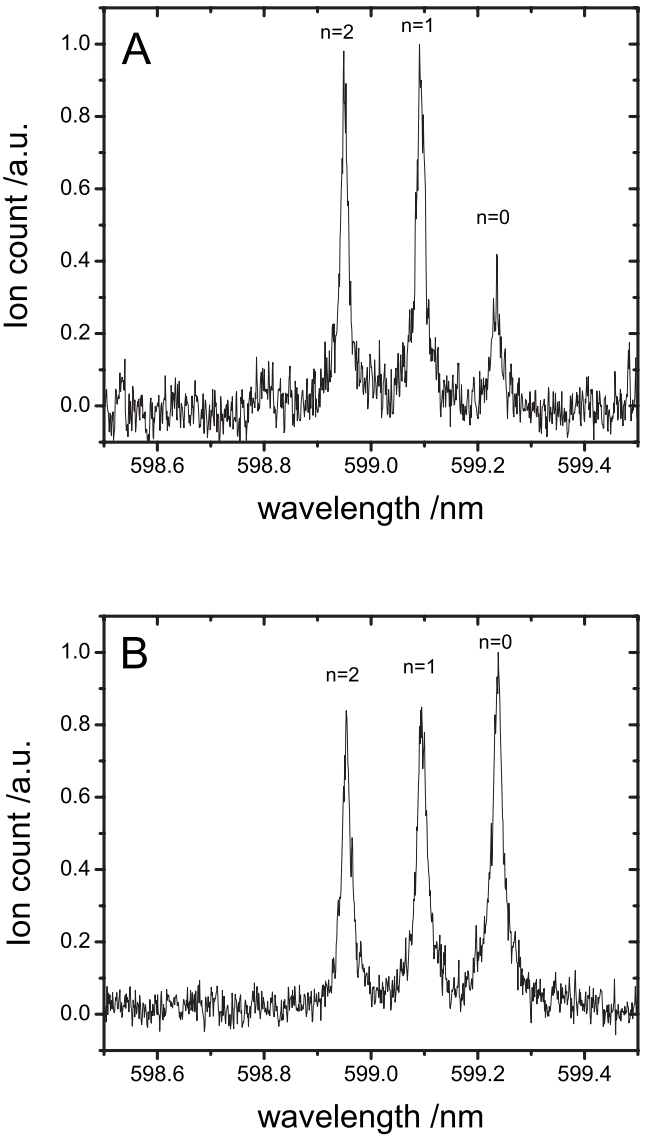

FIG. 5. Spectra taken with the dissociation laser fixed at the indicated resonance. (a) Transition 7 and (b) transition 4. The probe laser was scanned over the indicated rotational resonances $n=0$, $n=1$, and $n=2$.

C. Rotational state distribution spectra at a fixed dissociation wavelength

To determine the exact distribution of the excess energy over the rotational degrees of freedom of the NO(A,n) ions, the dissociation laser was kept fixed at a selected resonance and the probe laser was scanned over the NO($A,n=0,1,$and 2) levels. For the pump resonances labeled 4 and 7, these spectra are shown in Fig. 5. The distribution of excess energy over the rotational degrees of freedom of the NO(A) molecule are listed in Table II. The excess energy is defined as the photon energy of the dissociation laser minus the appearance energy. Transitions labeled 4–8 show a clear contribution of NO($A,n=2$).

However, the energetics show that these NO($A,n=2$) molecules are produced with more translational energy than expected implying they are formed from rotationally hot NO–Ar clusters, they have a positive $E_{int,cluster}$. Additionally we note that they appear at the energetic threshold for their

TABLE II. Rotational branching ratios of the above threshold resonances. The listed excess energy is the photon energy at the particular transition minus the appearance energy.

Peak	E_{exc} (cm^{-1})	$n=0$	$n=1$	$n=2$
2	−0.3	0.33	0.67	0.00
3	5.7	0.33	0.62	0.05
4	9.2	0.38	0.32	0.30
5	9.7	0.18	0.51	0.31
6	12.7	0.21	0.39	0.40
7	15.2	0.16	0.43	0.41
8	16.7	0.31	0.24	0.45
E_{rot} (cm^{-1})		0	4.0	12.0

production, peak 4 in Fig. 2 is at 44 304 cm^{-1}. These two observations give us a clue to how the NO(A,$n=2$) molecules are formed.

The observation that they appear at their energetic threshold implies that they cannot be formed by impulsive dissociation of a cold NO–Ar cluster. If a nonrotating NO–Ar cluster were to dissociate and in doing so creates an excited state NO($n=2$) molecule then some energy would have to go into translational recoil energy of the NO and Ar. A simple impulsive model shows that in order to deposit 12 cm^{-1} of rotational energy into the NO approximately 20 cm^{-1} of energy must be deposited into translational recoil energy.[24] This implies that if impulsive dissociation produced the molecules in the $n=2$ rotational state one should not observe the NO(A,$n=2$) molecules at the energetic threshold but about 30 cm^{-1} above the threshold, near 44 324 cm^{-1} in Fig. 2. The observation that the $n=2$ products have positive values of E_{int} shows that they are formed with only slightly more excess energy, 3 or 4 cm^{-1}, than the $n=0$ NO. This implies that they are not formed from $P'=2.5$ hotbands in the NO(X)–Ar cluster. It means the NO is not spinning in the NO(X)–Ar cluster and the NO(A,$n=2$) is not formed by impulsive dissociation.

In the following we hypothesize about the mechanism which produces the NO(A,$n=2$) molecules after excitation to the A state of the complex. Following electronic excitation there is sufficient mixing within the rotating cluster as it changes geometry from being T shaped in the NO(X)–Ar state to linear in the NO(A)–Ar state that only total energy, E, and total angular momentum, J, are good quantum numbers within the excited cluster. This mixing allows the low energy high angular momentum tumbling motion of the ground state NO(X)–Ar complex ($J'=4.5$ on average) to be converted into NO spinning motion ($P=2.5$ or greater) in the A state of the complex. This spinning complex then falls apart adiabatically producing NO(A,$n=2$) molecules at the energetic threshold. This indicates that the resonances can be attributed to some type of vibrational Feshbach resonance. Better calculations of the NO(A)–Ar potential and dissociation dynamics are clearly needed to better understand the NO(A,$n=2$) production.[25]

D. Angular distribution

Besides the radial distribution of the ion images the angular distribution also gives information about the long lived complexes, see Figs. 3(e) and 4(e). The argon atom in the NO–Ar complex lifts the cylindrical symmetry of the NO Π state. This effect gives rise to two potential energy surfaces A' and A'', which have an energy splitting of about 2.7 cm^{-1}, in which the A'' state is the lowest in energy.[7] The A'' surface is the state in which the unpaired electron occupies an orbital perpendicular to the plane of the complex and for the A' state the unpaired electron occupies an orbital parallel to the plane of the complex. The NO(A)–Ar state originates from NO(A, $^2\Sigma$) and only has A' symmetry. The NO(X)–Ar A' to NO(A)–Ar A' transition is parallel which results in a $\cos^2(\theta)$ distribution of the NO(A) fragments, with $\beta=2$ in the limit of fast axial recoil. The NO(X)–Ar A'' to NO(A)–Ar A' transition, however, is perpendicular and leads to a $\sin^2(\theta)$ distribution of the NO(A) fragments, with $\beta=-1$ in the limit of fast axial recoil. The ion images of the NO(A) fragment all show an anisotropic angular distribution with the intensity near the equator, indicative of a perpendicular transition, see Table I. There can be several explanations for this behavior. The transition could be via a parallel transition but the extreme bending associated with the change from T shaped to linear in the excited state causes the angular distribution to appear with a negative beta parameter. Another explanation is that the transitions giving rise to the resonant structures originate only from the A'' NO(X)–Ar potential energy surface. The decrease in the anisotropy parameter can be attributed to the lifetime of the NO(A)–Ar complex. The inhomogeneously broadened peaks in the action spectrum, see Fig. 2, have a width of about 2 cm^{-1} and each broadened line is the convolution of overlapping rotational hotband transitions. The average J value, of the NO(A)–Ar state, is estimated to be 4.5. If we assume that the inhomogeneous line width of 2 cm^{-1} is due to a convolution of some six transitions, each having a homogeneous line width of about 0.8 cm^{-1} ($\sqrt{(6)} \times 0.8$ $cm^{-1}=2$ cm^{-1}), this homogeneous width of 0.8 cm^{-1} corresponds to a lifetime $\tau \approx 13$ ps. Jonah[26] derived an expression calculating the reduction of the anisotropy parameter β for a perpendicular transition due to a rotation of the complex with angular frequency ω during a lifetime τ,

$$\beta = 2\left(\frac{-1/\tau\omega + \tau\omega}{2/\tau\omega + 8\tau\omega}\right). \tag{4}$$

In the limiting case that $\tau\omega \to 0$, $\beta=-1$ corresponding to a prompt perpendicular dissociation. The reduction of the anisotropy parameter listed in Table I corresponds to a product of $\tau\omega$ around 0.75, corresponding to a lifetime of 13 ps which is consistent with the linewidth of the transitions. Although this model is too simple to represent a definitive explanation, the reduction in the anisotropy and the order of magnitude of the lifetime needed for this reduction corresponds with an estimate of the lifetime derived from the line widths in the action spectra.

IV. CONCLUSION

We have employed direct excitation to the predissociative part of the NO–Ar A state followed by rotational state selective ionization of the NO fragment. Velocity-mapped ion imaging of the NO ion yields the recoil energy of this rotational state-selected fragment. The appearance energy for the formation of $NO(A,n=0)+Ar$ is found to be $44\,294.3 \pm 1.4$ cm^{-1}. A substantial contribution of rotational hotbands to the resonant structures is observed. The origin of the resonant structures in the spectrum of the predissociative part of the A state in the NO–Ar van der Waals cluster has been investigated and the resonances are attributed to Feshbach resonances involving bend and stretch of the NOAr(A) complex. The NO ($n=0$, 1, and 2) fragment velocities, obtained from analysis of the images, indicate that a centrifugal barrier is not responsible for the origin of the resonance transitions and that the $n=2$ products come from more rotationally hot clusters than does the $n=0$ fragments. The linewidth of the peaks observed in the action spectra and the decrease in the anisotropy of the fragments, are consistent with inhomogeneous broadening where each underlying transition has an estimated lifetime of the excited NO(A)–Ar cluster of about 13 ps.

ACKNOWLEDGMENTS

We gratefully acknowledge Mr. Mark Jaska for excellent technical help with this project. D.W.C., K.E.S., and C.C.H. acknowledge funding for this work provided by the U.S. Department of Energy, Office of Basic Energy Science. Sandia is a multiprogram laboratory operated by Sandia Corporation, a Lockheed Martin Company, for the U.S. Department of Energy. W.G.R. gratefully acknowledges the financial support from the EU by a Marie Curie Outgoing International Fellowship under Contract No. OIF 021907. W.G.R. acknowledges helpful discussions with Professor S. Stolte.

[1] E. A. Wade, K. T. Lorenz, D. W. Chandler, J. W. Barr, G. L. Barnes, and J. I. Cline, Chem. Phys. **301**, 261 (2004).
[2] A. Gijsbertsen, H. Linnartz, J. Klos, and S. Stolte, Phys. Scr. **72**, C1 (2005).
[3] B. F. Parsons, D. W. Chandler, E. C. Sklute, S. L. Li, and E. A. Wade, J. Phys. Chem. A **108**, 9742 (2004).
[4] K. Sato, Y. Achiba, H. Nakamura, and K. J. Kimura, J. Chem. Phys. **90**, 4961 (1986).
[5] K. Tsuji, K. Shibuya, and K. Obi, J. Chem. Phys. **100**, 5441 (1994).
[6] M. J. McQuaid, G. W. Lemire, and R. C. Sausa, Chem. Phys. Lett. **227**, 54 (1994).
[7] A. M. Bush, J. M. Dyke, P. Mack, D. M. Smith, and T. G. Wright, J. Chem. Phys. **108**, 406 (1998).
[8] N. Shafizadeh, Ph. Bréchignac, M. Dyndgaard, J. H. Fillion, D. Gauyacq, B. Levy, J. C. Miller, T. Pino, and M. Raoult, J. Chem. Phys. **108**, 9313 (1998).
[9] O. L. A. Monti, H. A. Cruse, T. P. Softley, and S. R. MacKenzie, Chem. Phys. Lett. **333**, 146 (2001).
[10] Y. Kim, J. Fleniken, H. Meyer, M. H. Alexander, and P. J. Dagdigian, J. Chem. Phys. **113**, 73 (2000).
[11] A. J. Alexander, Z. H. Kim, S. A. Kandel, T. P. Rakitzis, Y. Asano, and S. Yabushita, J. Chem. Phys. **113**, 9022 (2000).
[12] P. D. A. Mills, C. M. Western, and B. J. Howard, J. Phys. Chem. **90**, 4961 (1986).
[13] D. S. King, J. Chem. Phys. **82**, 3629 (1985).
[14] C. Zhu, N. Balakrishnan, and A. Dalgarno, J. Chem. Phys. **115**, 1335 (2001).
[15] J. C. Miller, J. Chem. Phys. **90**, 4031 (1989).
[16] D. J. Nesbitt, C. M. Lovejoy, T. G. Lindemann, S. V. ONeil, and D. C. Clary, J. Chem. Phys. **91**, 722 (1989).
[17] M. T. Berry, M. R. Brustein, and M. I. Lester, J. Chem. Phys. **92**, 6469 (1990).
[18] J. L. M. Desouter-Leconte and V. Brems, J. Chem. Phys. **103**, 4524 (1995).
[19] V. Brems and M. Desouter-Lecomte, J. Chem. Phys. **116**, 8318 (2002).
[20] H. H. W. Thuis, S. Stolte, J. Ruess, J. J. H. van den Biesen, and C. J. N. van den Meijdenberg, Chem. Phys. **52**, 211 (1980).
[21] D. W. Chandler and P. L. Houston, J. Chem. Phys. **87**, 1445 (1987).
[22] A. T. J. B. Eppink and D. H. Parker, Rev. Sci. Instrum. **68**, 3477 (1997).
[23] D. Proch and T. Trickl, Rev. Sci. Instrum. **60**, 713 (1989).
[24] H. B. Levenene and J. J. Valentini, J. Chem. Phys. **87**, 2594 (1987).
[25] J. Klos, M. H. Alexander, R. Hernandez-Lamondea, and T. G. Wright, J. Chem. Phys. **129**, 244303 (2008).
[26] C. Jonah, J. Chem. Phys. **55**, 1915 (1971).